LIVE EXPERIMENTS ON MELT POOL HEAT TRANSFER IN THE REACTOR PRESSURE VESSEL LOWER HEAD

Miassoedov A.*, Gaus-Liu X., Cron T. and Fluhrer B.
Karlsruhe Institute of Technology (KIT)
Eggenstein-Leopoldshafen, 76344
Germany

*Author for correspondence
E-mail: alexei.miassoedov@kit.edu

ABSTRACT

The main objective of the LIVE program at Karlsruhe Institute of Technology (KIT) is to study the core melt phenomena both experimentally in large-scale 2D and 3D geometry and in supporting separate-effects tests in order to provide a reasonable estimate of the remaining uncertainty band under the aspect of safety assessment. Within the LIVE experimental program several tests have been performed with water and with non-eutectic melts (mixture of KNO_3 and $NaNO_3$) as simulant fluids to study the heat flux distribution in the conditions when the melt pool is covered by water from the top.

The tests were performed in LIVE-3D and LIVE-2D facilities using different simulant materials and under different external cooling condition. The upward and downward heat transfer was compared between the 2D and 3D geometries. Although similar heat flux distribution through the vessel wall is observed for LIVE-3D and LIVE-2D tests, LIVE-2D test results have shown higher heat transfer from the top of the melt pool as compared to the LIVE-3D tests and to results from previous studies. Using water as simulant material resulted in a lower heat transfer both to the top of the pool and to the vessel wall. The outcomes of the LIVE top-cooling tests provide new insights for the evaluation of the established Nu-Ra correlations.

The results of these experiments allow a direct comparison with findings obtained earlier in other experimental programs (SIMECO, ACOPO, BALI, etc.) and are used for the assessment of the correlations derived for the molten pool behavior.

Besides the investigation of molten pool heat transfer behavior, melting process of debris in the reactor lower plenum after relocation of liquid melt in a large scale hemispherical geometry is also investigated in LIVE-3D facility using a non-eutectic nitrate to simulate the debris bed material. Two experiments have been performed with different volume of the relocated liquid melt. The onset of melting, the form and the volume of the melt pool and the timing of important events during the melting process were identified.

INTRODUCTION

The in-vessel melt retention (IVR) by flooding the reactor vessel wall externally is regarded as an effective severe accident management strategy [1]. The effectiveness of this method depends on whether the local heat flux from the melt pool through the wall is lower than the critical heat flux (CHF) of the external cooling water. Water injection into in the reactor pressure vessel to cool the melt from the top could be an additional mitigation strategy to reduce the thermal loads on the pressure vessel wall. Certainly, other responses of these measures such as steam and hydrogen production and the possibility of pressure increase should be evaluated. On the other hand, a two-layer melt pool can be formed at a certain melt composition if a metallic layer is atop of an oxide layer [2]. A high heat transfer coefficient from the oxide layer upwards to the metallic layer can taper the heat flux at the metallic layer, thus transfer the critical thermal load to the metallic layer.

Numerous experimental and analytical studies have been already performed to characterize the upward and downward heat transfer from the oxide melt pool. The experimental studies were performed in different geometries (3D or 2D), using different simulant materials (water, salts and prototypical corium melts) and boundary cooling conditions and simulation of the internal heat sources (direct electrical heating, inductive heating, microwave, transient cooling etc.) [3]-[8]. The question is how predictive are the results obtained from different experimental geometries, boundary conditions or simulant materials?

The objective of the study at KIT is to perform a series of top-cooling tests in LIVE-3D and LIVE-2D facilities in order to compare the results from hemispheric and semi-circle geometry and from different simulant melts. The LIVE-3D and LIVE-2D test vessels have the same diameter of the test section of 1 m.

In the tests, the same simulant material (a non-eutectic mixture of 20 mol % $NaNO_3$-80 mol % KNO_3), same heating method (electrical resistance heating wires) and same cooling condition are used [9]-[11]. Besides the characterization of heat flux distribution, the upward to downward heat flux ratio from the melt pool is the main interest of the study.

NOMENCLATURE

c_p	[J/g/°C]	thermal capacity
g	[m/s²]	gravitational acceleration
H	[m]	pool height
ΔH_{tr}	[J/g]	enthalpy of phase transition
ΔH_{fus}	[J/g]	enthalpy of fusion
L	[K]	characteristic length in Nu and Ra_i
Nu	-	Nusselt number
q	[W/m²]	heat flux
Ra_i	-	internal Rayleigh number
$\dot{q}$	[kW/m³]	power source density
Pr	-	Prantl number
T	[K] / [°C]	temperature
Q	[W]	rate of heat input or heat transfer
V_{pool}	[m³]	volume of melt pool

Special characters

α	[m²/s]	thermal diffusivity
β	[1/K]	thermal expansion coefficient
θ	[°]	polar angle of the vessel wall lower head
λ	[W/(mK)]	thermal conductivity
v	[m²/s]	kinematic viscosity
ρ	[kg/m³]	density
α	[m²/s]	thermal diffusivity

Subscripts

in	input
$mean$	global mean value of the vessel wall
dn	downward heat transfer
int	interface
liq	Liquidus , liquid state
max	maximum
p	at the position of the pool surface
tr	phase transition
up	upward heat transfer
w	heat transfer through the vessel wall

EXPERIMENTS

Test facility description

The LIVE 3D test vessel represents a hemispherical lower plenum of a reactor pressure vessel (RPV) of a pressurized water reactor (PWR) in 1:5 scale [12], [13]. The melt surface can be either free surface by covering the test vessel with an insulation lid [14], [15] or cooled with a water-cooling lid. The test vessel with the top cooling lid is shown in **Figure 1**. Both the test vessel and the top cooling lid are made of stainless steel SS316Ti. The inner diameter of the test vessel is 1 m and the wall thickness is ~25 mm. The test vessel is enclosed in a cooling vessel to enable external cooling with either water or air. The cooling water for the side wall cooling anters the cooling vessel at the bottom, the outlet is located at the top of the cooling vessel. There are four peripheral water inlets and one central outlet at the cooling lid. The cooling lid has a

diameter of 92 cm and is mounted at height 41.3 cm from the vessel bottom. There is a narrow gap of about 3.6 cm between the cooling lid and the vessel wall. The water flow rate for the external cooling and for the top cooling are controlled separately. The decay heat in the melt is simulated by 8 planes of electrical resistance heating wires, which can be controlled separately to realize homogenous power generation in the melt pool. The distance between the heating planes and between the windings is 45 mm. The maximum possible homogenous heat generation is 29 kW. The liquid simulant melt is prepared in the external heating furnace, which can be tilt to pour the liquid melt into the test vessel either centrally or near to the vessel wall using a pouring spout.
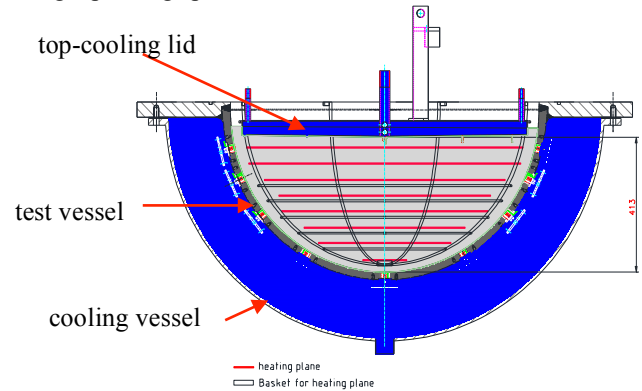

Figure 1 LIVE-3D test vessel with the top-cooling lid

The LIVE-3D test vessel is extensively instrumented. Melt pool temperatures are measured with 57 thermocouples distributed homogeniously in the melt. 17 pairs of thermocouples are mounted on the vessel inner and outer surface at polar angles of 0°, 30°, 51°, 65° and 76.5° and at four azimuthal orientations. The wall temperatures enable the determination of the downwards heat flux distribution through the vessel wall. Crust solidification process along the vessel wall is monitored by 3 thermocouple trees at polar angles 37.6°, 52.9° and 66.9°. Two video cameras are installed to detect the melt pouring process. The vessel is placed on three weighting cells, so that the weight changes during melt pouring and melt extraction can be controlled. Detailed description of the instrumentation is given in [9]

The LIVE-2D test vessel is a slice which is also 1:5 scaled to the reactor pressure vessel. The inner diameter of the test vessel and the wall thickness are the same as the LIVE-3D vessel and the width of the slice vessel is ~12 cm. The front and the back walls of the slice are made of stainless steel and are insulated to reduce the heat losses, as it is shown in **Figure 2**. The test vessel can be cooled externally and from the top. For the external cooling the water flows from the bottom upwards to the left and to the right sides. For the LIVE-2D top cooling experimens a rectangular cooling lid is mounted at the height of 46 cm. The water flows from the center to the sides of the cooling lid. To simulate the homogenious heat generation by the decay heat the heating elements can be controlled separately and allow a homogeneous heat generation rate of maximum 13 kW [10].

Figure 2 LIVE-2D test vessel with side walls (top) and with the view of heaters (bottom)

The LIVE-2D test vessel is instrumented with 13 thermocouples in the melt and 10 pairs of thermocouples on the vessel wall inner and outer surface. Crust formation and growth is monitored by numerous thermocouple trees intruding from the inner wall into the melt at 6 different locations.

The LIVE-3D and LIVE-2D facilities use the same heating furnace for the preparation of the melt and its discharge into the test section. The simulant melt is heated to 350 °C in the heating furnace before it is poured into a test vessel. One test phase at one heat generation rate is terminated when the thermodynamic steady state of the melt pool is approached. At the end of each test, the residual melt is extracted back to the heating furnace via a vacuum pump.

A non-eutectic binary mixture of 20 mol% $NaNO_3$-80 mol% KNO_3 composition is selected as simulant material of corium for the LIVE tests. According to own measurements [16], the solidus temperature of this mixture is about 223 °C and the liquidus temperature is about 284 °C. Other physical properties of the simulant are given in **Table 1**.

Table 1 Thermal-physical properties of 20 mol% $NaNO_3$-80 mol% KNO_3.

		unit	solid	liquid
c_p	thermal capacity	J/g/°C	0.9474+0.00113·T (°C) (119°C<T<182°C) [KIT measurement]	1.2475+2.8E-4·T(°C) (300°C<T<400°C) [KIT measurement]
ρ	density	kg/m³	2.1-2.26 [KIT measurement]	1.914 at 284°C; 1.873 at 340 °C [17]
T_{tr}/ T_{liq}	Transition/ liquidus temperature,	°C	104.8 [KIT measurement]	284.4 [KIT measurement]
ΔH_{tr}/ ΔH_{fus}	Transition/ fusion enthalpy,	J/g	65.7, 60°C-118°C [KIT measurement]	161.96 at 220°C-286°C [KIT measurement]
ν	kinematic viscosity,	x10-6m²/s	-	1.75 at 300°C; 1.35 at 350°C [17]
β	thermal expansion rate	x10-4/K,		3.81 [17]
λ	themal conductivity	W/(mK)	0.4-0.6 [KIT test data]	0.439 at 300°C 0.422 at 350°C [17]

Test programm

Three experiments with cooling the melt from the top were carried out in the LIVE-3D facility. The test conditions were different regarding the simulation material and the cooling conditions. As it is shown in the **Table 2**, 20% $NaNO_3$-80% KNO_3 mixture was used as the simulant material in the L7V and L7TC tests, whereas water was used as a simulant material in the L7W test. During the L7V and L7W tests both the top cooling surface and the external cooling of the vessel wall were performed. In the L7TC test only the upper surface of the melt was cooled and no external water cooling at the vessel wall was activated. The water flow inlet and outlet temperature differed by ~10°C, so that the temperature difference is large enough for an accurate calculation of heat removed from the top and from the side of the vessel. Four power generation rates were applied in all three tests in the same order. The melt pool height in the LIVE-3D tests was kept 1-2 cm above the lower plate of the cooling lid to insure a good contact between the melt pool and the cooling lid.

Table 2 Test programme of top-cooling test in LIVE-3D and LIVE-2D facilities

LIVE-3D	**cooling conditions**		**power [kW]**
	upper lid	**vessel wall**	
L7V (salt test)	water	water	29->24->18->9
L7W (water test)	water	water	29->24->18->9
L7TC (salt test)	water	No water cooling	29->24->18->9
LIVE-2D	**upper lid**	**vessel wall**	**power [kW]**
L00A1	water	water	7.3->6.3->4.2
L01	water	water	7.3->3.7->7.3
L02	water	water	3.7->7.3->3.7

To compare the results to the 2D geometry, three top-cooling tests under similar conditions were performed in the LIVE-2D facility. Both the melt surface and the vessel wall were water-cooled in these tests. Three levels of power input were realized during each test. The tests differed only in the order of the power plateaus. The melt pool height in LIVE-2D tests was 46 cm.

MOTLEN POOL BEHAVIOUR

Melt temperature and heat flux profiles of LIVE-3D tests

The melt temperature vertical distribution measured at the radius of 3 cm is shown in **Figure 3**. For the tests with external cooling (L7V and L7W) the melt pool has a lower zone with temperature stratification and a well-mixed upper zone. However, the proportion of the two zones and the temperature gradient at the lower zone are different. The melt temperatures are normalized in terms of $\Delta T/\Delta T_{mean}$, with

$$\Delta T = T - T_{int} \text{ and } \Delta T_{mean} = T_{mean} - T_{int}$$

The normalized temperature distribution is shown in **Figure 3** (d). Comparing the salt test L7V with a uniform interface temperature, $T_{int} = T_{liq}$, the water test L7W has a higher temperature gradient in the lower zone and a larger well-mixed upper zone. The upper part of the pool in water test is located at $H/H_p > 0.4$ whereas in salt test it was detected at $H/H_p > 0.7$. The location of the upper zone is compared with the results obtained in other facilities. Using water as a simulant material, the lower boundary of the upper zone H/H_p is 0.6 in the SIMECO test [6], in the BALI test the H/H_p is about 0.5 [4]. It should be noticed that both SIMECO and BALI tests were performed in a 2D geometry.

In the water test L7W the temperature near the bottom of the pool was lower than the average interface temperature T_{int}. In the salt test L7V, the temperature at the pool bottom should be lower than the interface temperature due to the crust formation. However, due to the lowest heating plane in the LIVE-3D facility, the melt temperatures show higher values. The melt temperature near the top surface is about 1.2 times the global mean melt temperature for both the salt test and the water test.

The different temperature profiles between the water test and the salt test can be caused by a number of reasons. The material properties in terms of the Prandtl number can be a major one. The Pr of the nitrate salt is in the range of 8-10; the Pr of water is between 2.8 and 4. Moreover, the crust formation can influence the interface temperature between the melt and the crust to be uniform and equal to the liquidus temperature, but this assumption cannot be fully certified. In the BALI water experiments the cooling concept enabled ice formation at the vessel wall. Nevertheless, the temperature profile was similar to the profile observed in the L7W test.

In the experiment without external water cooling (L7TC) the melt temperature is almost isothermal as it is shown in the **Figure 3** (b). Generally the temperature was ~10°C higher than the maximum melt temperature measured in the L7V, however it was ~27°C lower than the maximum temperature of a melt pool with an insulated top lid [15].

The horizontally averaged heat fluxes are shown in the **Figure 4**. The main source of the uncertainty is the system error of the thermocouples mounted at the wall inner and outer surface. The system error is comparatively large for low heat fluxes. The scattering range of local heat fluxes at one horizontal level and different azimuthal orientation is about 8-16 %. Generally, the heat flux in the salt test L7V is higher than in the water test L7W. In the L7V test the heat flux measured below a polar angle of 30°C was constant or even decreased along the polar angle, and was increasing linearly above this position. In the water test the heat flux increased from the bottom to the polar angle of 50° and kept constant above this position.
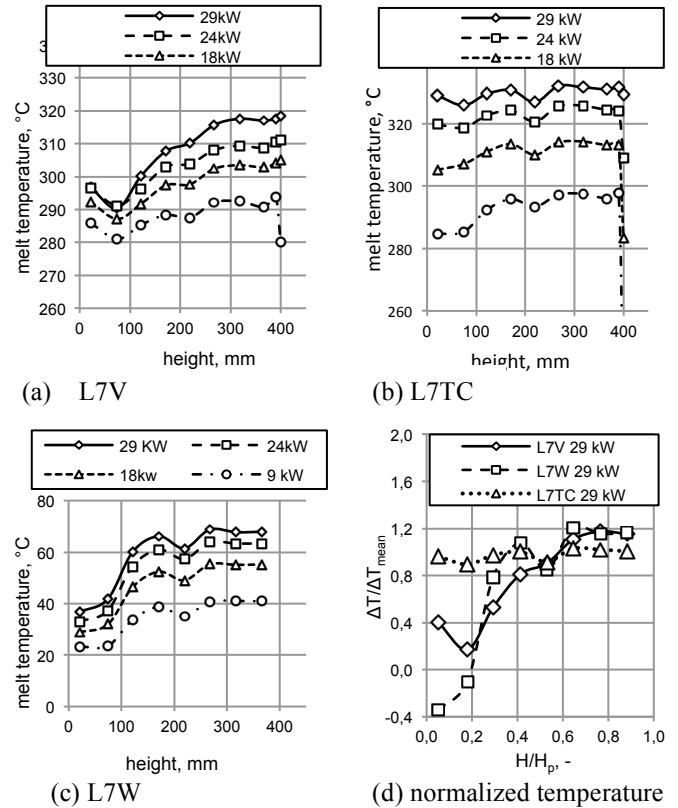

(a) L7V   (b) L7TC

(c) L7W   (d) normalized temperature

Figure 3 Melt temperature distribution in the L7V test (a), L7TC test (b), L7W test (c) and normalized temperature of three tests (d)
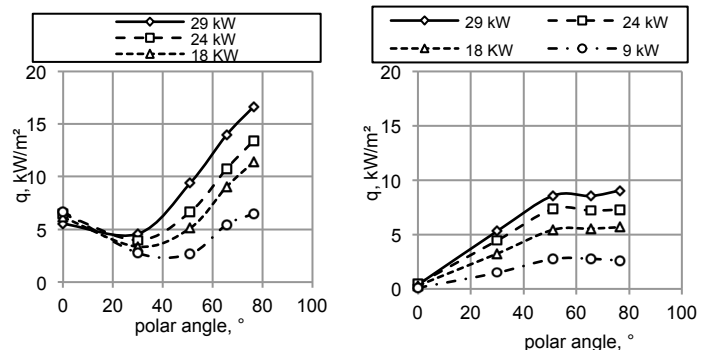

Figure 4 Heat flux profiles along the vessel wall of L7V test (left) and L7W test (right)

The normalized heat flux values weighted by the area-mean heat flux, q/q_{mean}, are shown in the **Figure 5**. The maximum heat flux in the salt test is about 1.7 times and in water test 1.3 times higher than the mean value. The q_{max}/q_{mean} ratio is compared to other studies. In salt test, SIMECO´s value was 1.7 both for eutectic and non-eutectic salt [6]. There are larger differences in water tests. In the mini-ACOPO [7] and BALI tests, q_{max}/q_{mean} is about 1.7 [4], whereas in SIMECO it is 1.3. In the study of Jahn and Reinecke [5] the q_{max}/q_{mean} of experimental results is between 1.9-2.0 for semi-circular geometry.
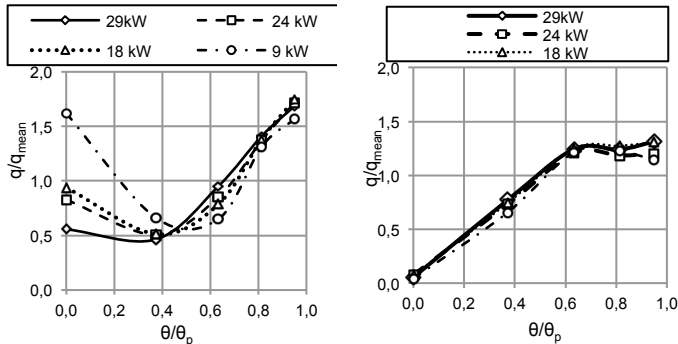

Figure 5 Normalized heat flux profiles of L7V (left) and L7W (right)

Heat flux and melt temperature profiles of LIVE-2D tests

The aim of LIVE-2D tests is to compare the melt behaviour between hemispheric and semi-circular geometries. Concerning the top cooling condition two salt tests with similar power source densities were selected for the comparison: the LIVE-3D L7V test with 18 kW power generation rate and the LIVE-2D with 3.7 kW power generation rate. The power densities in the LIVE-3D L7V 18 kW and LIVE-2D 3.7 kW are 92 kW/m³ and 88 kW/m³ respectively.

The normalized melt temperature and heat flux profiles are shown in the **Figure 5**. Both the melt temperature distribution and the heat flux in the LIVE-2D test demonstrate similar profiles compared to the LIVE-3D tests. In the upper part of the melt pool the normalized melt temperatures and heat fluxes in LIVE-2D tests were slightly higher than the results in LIVE-3D tests: $\Delta T_{max}/\Delta T_{mean}$ is 1.2 and the q_{max}/q_{mean} is about 1.9. Based on the similar q_{max}/q_{mean} a general conclusion can be drawn that for isothermal cooling condition at the top of the melt pool and at the vessel wall, and with Pr number of the melt about 7, the maximum heat flux is about 1.7-1.9 times higher than the average heat flux. This maximum to average value can be used for Ra_i number between 10^8-10^{13}. Comparing a melt pool without top cooling, e.g. the LIVE-L10 test [15] having the ratio of q_{max}/q_{mean} between 2.3 to 2.5 the top cooling concept is very beneficial for oxide pools. Since the top-cooling concept not only extracts a large part of the decay heat, but also reduces the tapering of the heat flux near the melt upper surface.

Despite of the similarity of the distribution characteristics between semi-circular and hemispheric geometries through the curved vessel wall, significant differences are observed concerning the heat transfer to the top surface and through the sidewall, which can be shown in the following description of the top/side heat transfer ratio and the Nusselt number.
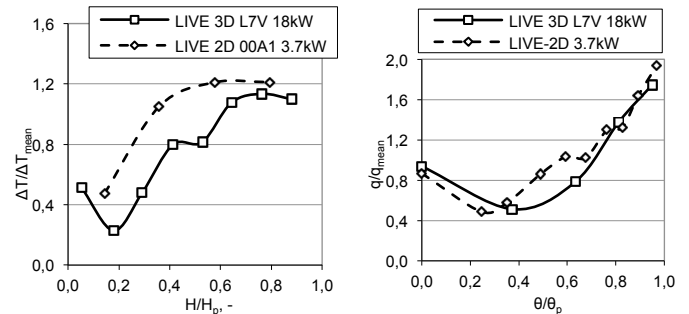

Figure 6 LIVE 3D and LIVE 2D comparison of normalized melt temperature (left) and heat flux (right)

Energy balance, top/down heat transfer ratio

The energy balance between the power input and the heat extracted from the melt by the top cooling and the external cooling was examined. In the Table 3 and 4 the heat transfer data of LIVE-3D tests and LIVE-2D tests are given respectively. A total heat transfer ratio is defined as Q_{out}, which is the sum of the heat removed by the cooling water from the sidewall Q_w and from the top cooling lid Q_{up}. For the LIVE-3D L7V and L7W tests the total heat transfer rate is about 0.85. For the L7TCt est, this rate is lower since there was no water cooling at the vessel wall and the heat transfer through the vessel wall was not considered. In the LIVE-2D test the total heat transfer ratio is about 1.

The heat losses in the LIVE-3D facility are due to the thermal radiation and the heat convection from the melt surface to the environment at the gap between the top lid and the vessel wall. The melt surface area at the gap which amounts to about 12% of the total melt surface area, could have a significant contribution to the total heat loss. In the LIVE-2D tests the gap between the cooling lid and the vessel wall is smaller than in the LIVE-3D facility and it was filled with crust during the whole test period. The main interest of the study, the top to sideward heat flux ratio q_{up}/q_{dn} are compared between the LIVE-3D and the LIVE-2D tests. The average value of q_{up}/q_{dn} in the L7V test is 1.7 and in the L7W test is 1.2. In the LIVE-2D facility this number was significantly higher and amounted to 3.4. This means that the heat flux split ratio in the LIVE-2D is twice as higher as in the LIVE-3D tests. The top/down heat flux ratio in L7V is 3.7 in average whereas in LIVE-2D it is 5.1 in average. The LIVE-2D test results imply a much stronger upward heat transfer in 2D than in 3D geometry.

Table 3 LIVE-3D tests energy balance and top/down heat transfer ratios

	$\dot{q}$	Q_{in}	(Q_{out}/Q_{in})	Q_{up}/Q_{dn}	q_{up}/q_{dn}	Ra_i x10^13	Nu_{dn}	Nu_{up}
	kW/m³	kW	-	-	-		-	-
LIVE-L7V	148	29.2	0.82	1.7	2.3	5.4	221	642
	123	24.2	0.86	1.9	2.6	4.3	244	621
	92	18	0.83	1.9	2.2	3.2	231	519
	47	9.2	0.83	1.5	1.6	1.6	221	451
LIVE-L7W	148	29.1	0.85	1.4	3.2	2.0	164	600
	124	24.1	0.86	1.2	2.9	1.7	152	519
	92	18	0.83	1.1	2.8	1.2	120	448
	46	8.9	0.84	1	2.6	0.59	111	377
LIVE-L7TC	148	29.1	0.82			5.5		746
	123	24.2	0.8			4.5		708
	91	18	0.73			3.2		677
	46	9	0.58			1.6		615

Table 4 LIVE-2D tests energy balance and top/down heat transfer ratios

	L00A1-P1	L00A1-P2	L00A1-P3	L01-P1	L01-P2	L01-P3	L02-P1	L02-P2	L02-P3
$\dot{q}$, kW/m³	174	149	100	174	88	174	88	174	88
Q_{in}, kW	7.3	6.3	4.2	7.3	3.7	7.3	3.7	7.3	3.7
Q_{out}/Q_{in}	0.97	1.00	0.88	1.02	0.96	1.01	0.93	1.06	0.97
Q_{up}/Q_{dn}	3.4	3.2	4.9	2.9	3.8	2.8	4.2	2.4	3.1
q_{up}/q_{dn}	5.1	4.8	7.3	4.3	5.6	4.2	6.2	3.6	4.6
Ra_i, x10^13	12	9.8	6.0	12	5.3	12	5.3	12	5.3
Nu_{dn}	191	195	115	217	146	216	135	272	187
Nu_{up}	960	932	871	911	832	874	852	976	898

Nusselt numbers

The upward and downward Nusselt numbers are calculated according to the Equation (1)

$$Nu = \frac{qL}{(T_{max} - T_{int}) \cdot \lambda} \qquad (1)$$

Here q is the average heat flux through the vessel wall or through the top-cooling lid, L is the height of the melt pool without considering the crust thickness at the vessel bottom and the T_{max} is the maximum melt pool temperature.

In the salt test L7V and in all LIVE-2D tests the T_{int} is the liquidus temperature of the melt. Thus the T_{int} is uniform for all melt boundaries in salt tests. In the water test L7W the T_{int} is the average inner surface temperature for the sidewall and the average temperature at the downside of the bottom plate for the cooling lid. The T_{int} for the cooling lid is higher than the T_{int} for the vessel wall in the water test. For salt test, the Pr number is in the range of 8-11 and for water test Pr is between 2.5-4.

The internal Rayleigh number is calculated according to the Equation (2):

$$Ra_{in} = g.\beta \cdot q_i \cdot L^5 /(\nu \cdot a \cdot \lambda) \qquad (2)$$

The upward and downward Nusselt numbers in relation to the internal Rayleigh number are shown in **Figure 7**. For comparison, the results of previous studies for similar Rayleigh number range, such as SIMECO [6], mini-ACOPO [7], Asfia and Dhir [18], Mayinger [19] and Steinberner and Reinecke are also shown in **Figure 7**. The Ra-Nu correlations and applying Ra number range of the studies are given in **Table 5**.

Except the SIMECO experiments all other correlations come from experiments using water as simulant material.
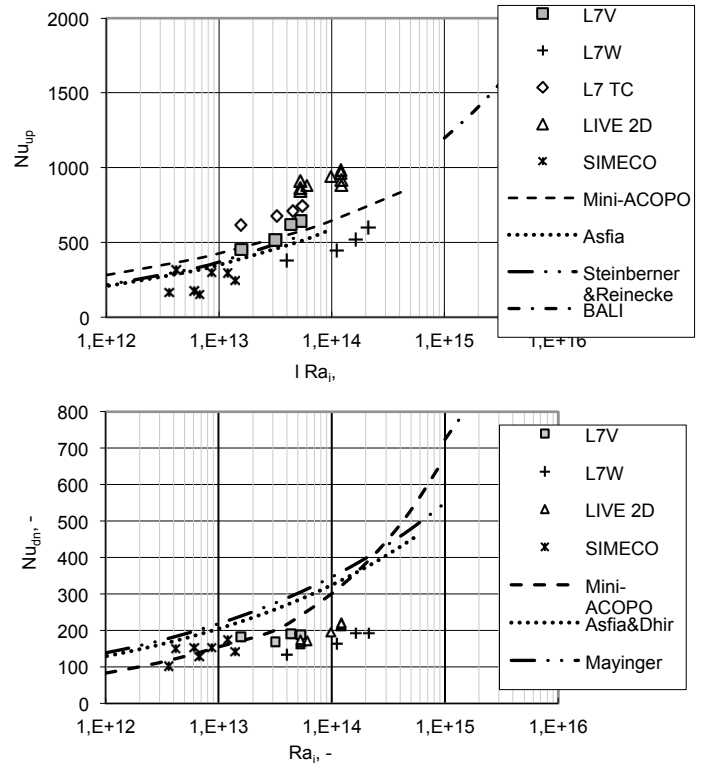

Figure 7 Comparison of upward Nusselt number (top) and downward Nusselt number (bottom) of LIVE-3D, LIVE-2D and previous studies

The upward Nusselt number obtained in the LIVE salt test L7V is in the same order of the magnitude as in other studies. However, the L7TC test and especially all LIVE-2D tests have shown higher upward Nusselt number. The Nu_{up} obtained in LIVE-2D experiments is 30% higher than predicted by other correlations. On the contrary, the Nu_{up} obtained in the water test L7W is lower than predicted by other correlations.

Considering the downward Nusselt number in the salt tests, an opposite trend is observed. LIVE-2D salt tests have lower value than L7V and other studies.

Table 5 Summary of the Ra-Nu ratio obtained in the hemispheric (3D) and in the semicircular (2D) geometry

Ref	Nu	Ra_i	Pr	Geometry	Upper Surface	Simulant
Mayinger [19]	$Nu_{up} = 0.36 Ra_i^{0.23}$ $Nu_{dn} = 0.54 Ra_i^{0.18}$	E7-E11	7	2D H=R	Cooled (isothermal)	-
ACOPO [8]	$Nu_{up} = 1.95 Ra_i^{0.18}$ $Nu_{dn} = 0.3 Ra_i^{0.22}$	E16	7-11	3D, R=2 m H=R	Cooled, transient cooling	Water
Mini-ACOPO [7]	$Nu_{up} = 1.95 Ra_i^{0.18}$ $Nu_{dn} = 0.038 Ra_i^{0.35}$, $E12 < Ra_i < 3E13$ $Nu_{dn} = 0.048 Ra_i^{0.27}$, $3E13 < Ra_i < 7E14$	E12-7E14	7-11	3D, R=0.4 m H=R	Cooled, transient cooling	Water, Freon-113
ULCA [1] Asfia&Dhir [18]	$Nu_{dn} = 0.55 Ra_i^{0.2}(H/R)^{0.25}$ $Nu_{up} = 0.403 Ra_i^{0.226}$	2E11-E14	8	3D R1=0.4 m R2=0.6 m H/R=0.5-1	Cooled rigid wall and insulated rigid wall	Water, ethanol, olive oil, Freon-113
BALI and COPOII-AP [4]	$Nu_{up} = 0.383 Ra_i^{0.233}$ $Nu_{dn,3D} = 0.131(H/R_{v,2D})^{0.19} Ra_i^{0.25}$ $Nu_{dn,2D} = 0.116(H/R_{v,3D})^{0.32} Ra_i^{0.25}$, $R_{v,2D} = (4V_{pool}/\pi L)^{1/2}$ $R_{v,3D} = (3V_{pool}/2\pi)^{1/3}$	E15-E17	8	BALI: 2D R=2 m COPO: 2D R=2 m	Cooled and free surface	BALI: Water COPOII-AP: H2O+ZnSO4

[1] Nu_{dn} is ±17% of the UCLA correlation for both surface insulation and cooling situations, Nu_{up} is taken from Kulacki&Emara

The ratio of Nu_{up}/Nu_{dn} was also evaluated and is shown in the **Figure 8**. For salt tests the Nu_{up}/Nu_{dn} ratio is identical to q_{up}/q_{dn} due to uniform interface temperature T_{int}; whereas in the water test a certain deviation to q_{up}/q_{dn} could be observed. In LIVE-3D tests, the Nu_{up}/Nu_{dn} ratio is about 3, whereas in LIVE-2D tests this ratio is between 4 and 5. In SIMECO and mini-ACOPO tests the Nu_{up}/Nu_{dn} ratio is about 2. There is also a general statement in [20] that Nu_{up}/Nu_{dn} is ~2 and the proportion of the decay power transferred to the top of the melt pool is ~50 %. In the study of Mayringer [19] for experiments in semicircular geometry for Ra number of 10^7-10^{11} a trend of increasing the Nu_{up}/Nu_{dn} ratio with the increase of the Ra number is obtained.
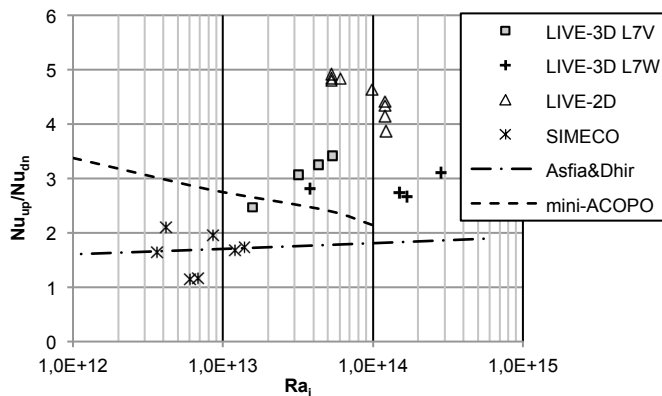

Figure 8. Nu_{up}/Nu_{dn} in LIVE-3D, LIVE 2D and other studies.

The beneficial effect of top cooling by relieving the thermal load of vessel wall at the oxide pool was already discussed. However, a strong upward heat transfer also means that more heat will be transferred to the metallic layer atop of the oxide layer in the case of a stratified melt pool configuration. Higher Nu_{up}/Nu_{dn} ratio in this case can result in higher heat flux at the vessel wall at the metallic layer increasing the focusing effect.

DEBRIS MELTING BEHAVIOUR

The debris melting process after the melt relocation from the core region into the lower plenum was investigated in two tests with different fractions of relocated liquid melt in LIVE-3D facility [21]. In the L8A test 70 vol. % of the liquid melt and in the L8B test 50 vol.% of the liquid melt were poured into preheated debris bed. Both the liquid melt and the debris particles were simulated by a 20% $NaNO_3$-80% $NaNO_3$ mixture. The particles size is in range of 3.5 -16 mm and the porosity is ~0.5. The maximum temperature of the preheated debris bed was slightly below the solidus temperature of the mixture. The temperature of the liquid melt is 350 °C. The heating power was switched to 21 kW after the melt pouring and maintained constant through the whole test duration. The total mass of the debris and the liquid melt was 351 kg corresponding to 406 mm pool height when totally molten pool.

In the **Figure 9** the melt temperature distribution during the preheating phase and after the melt relocation in the L8B test is shown. During the preheating period the maximum debris temperature was measured at the upper-centre region. After the melt relocation the voids in the debris bed were filled with liquid melt and an essential fraction of liquid melt was solidified in the lower part of the debris bed.
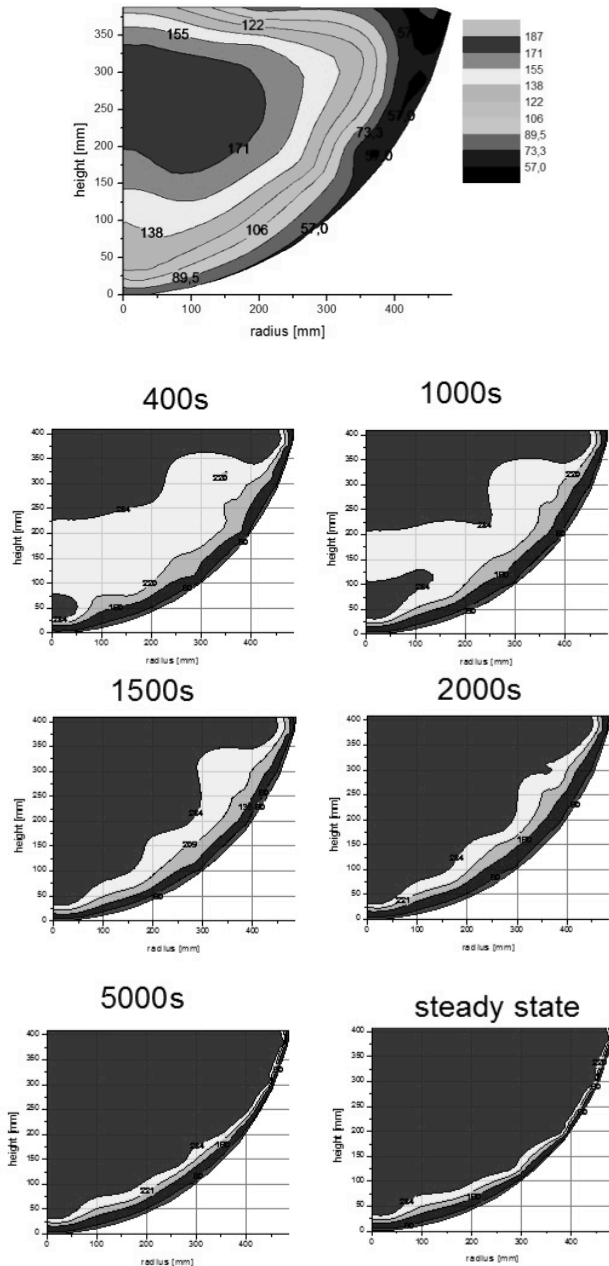
Figure 9. melt temperature distribution during L8B test. Top: preheating phase; bottom: after the melt relocation

The progression of the liquid in the two tests is shown in the **Figure 10**. The fraction of the liquid melt was reduced to 0.27 and 0.53 after the melt relocation in the L8B and L8A tests respectively. At about 10000 sec after the melt relocation the melt volume and the form of the melt pool approached the thermal-hydraulic steady state in which 90 vol. % of the whole inventory was molten. The difference in the pouring mass of the liquid melt only affects the initial liquid mass in the debris bed and the duration of the transient state and has a small influence on the steady state. A crust layer was formed having similar thickness compared to the crust layer formed directly from the solidified melt. However, in the debris melting tests a

loose debris layer remained at the bottom of the vessel during the whole test period.
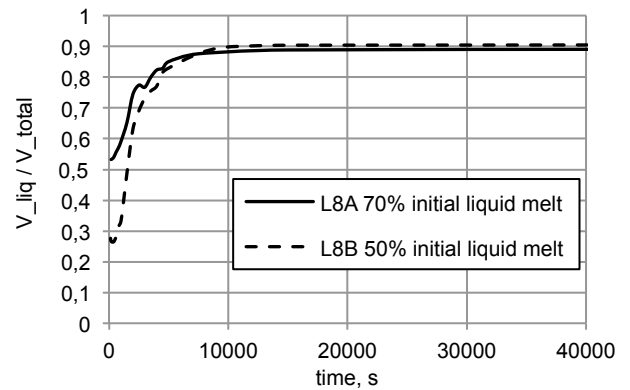

Figure 10 Progression of the liquid pool volume fraction after the melt relocation

The heat flux distribution through vessel wall during the L8A experiment is shown in **Figure 11**. The reduction of the heat flux after the melt pouring followed by a slight increase corresponds to the solidification of the poured liquid melt and the subsequent re-melting process. After 1000 s the heat flux through the vessel wall became stable.
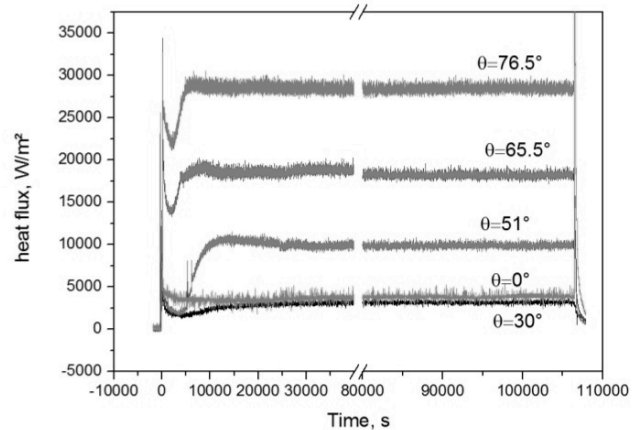

Figure 11 Heat flux through the vessel wall at the polar angle θ during the L8A experiment

CONCLUSION

Cooling the melt pool in the RPV from the top as an additional mitigation method of IVR that can effectively reduce the maximum melt temperature and the maximum heat flux through the vessel wall for oxide melt pool given that possible negative effects such as steam and hydrogen generation can be managed. However, the top cooling also implies a higher heat flux from the metallic layer atop of the oxide layer. The decay power transported to the top amounts to ~63% of the total power input as obtained in LIVE-3D results and even to ~77% in LIVE-2D results. These values are higher than obtained in

previous studies. Higher upward heat transfer obtained in the LIVE tests provides new insights and requirements for the examination of the established Nu-Ra correlations obtained for different Ra number range, simulant material and/or heating method.

LIVE-2D test results have similar melt temperature and heat flux distribution characteristics as LIVE-3D results. The maximum heat flux is about 1.7-1.9 higher than the average heat flux.

Use of water as simulant melt has shown a lower heat transfer coefficient compared to molten salt both to the top surface and to the curved vessel wall. Also the proportion of the lower stable zone to the upper well-mixed zone is different compared to the salt melt pool. The reason can be explained by the different Prandtl number of the simulant material and different boundary conditions.

The global debris melting process after the melt relocation to the lower head of the RPV is characterized by initial solidification of the liquid melt and the subsequent remelting process. The liquid pool boundary expands preferably towards the sidewall. After ~10000 s the melt temperature pool boundary and the heat flux through the vessel wall approach thermal-hydraulic steady state and the volume of the liquid melt reached ~90% of the whole pool volume regardless the initial pouring mass of liquid melt. The duration of the melting process lasted about 15000 s.

The liquid melt has reached the upper part of vessel wall after pouring, whereas a loose layer of debris remained at vessel bottom during the test period.

REFERENCES

[1] B. Sehgal and T. Dinh, "In-vessel melt retention (IVMR) as a severe accident management (SAM) Strategy," in *Severe accident phenomenology short course*, Cadarache, 2006.

[2] V. Asmolov, S. Bechta, V. Khabensky, V. Gusarov and V. Vishnevsky, "Partitioning of U, Zr and FP between molten oxidic and metllic corium," in *MASCA Project (2000-2003)/Vol.1. Proc. of the MASCA Seminar, 10–11 June 2004*, Aix-en-Provence, France, 2004.

[3] V. Asmolov, S. Abalin, A. Surenkov, I. Gnidoi and V. Strizhov, "Results of Salt Experiments Performed during Phase I of RASPLAV Project, RP - TR - 33," Russian Research Centre, 1998.

[4] J. Bonnet and J. Seiler, "Thermal hydraulic phenomena in corim pools: the BALI Experiment," in *7th ICONE*, Tokyo Japan, 1999.

[5] M. Jahn and M. Reinecke, "Free convection heat transfer with internal heat sources calculations and measurements," in *Proceedings of the 5. International Heat Transfer Conference, Vol. 3, p. 74*, 1974.

[6] G. Kolb, S. Theerthan and B. Sehgal, "Experiments on in-vessel melt pool formation and convection with NaNO3-KNO3 salt mixture als simulant," in *Proceedings of ICONE 8*, Baltimore, USA, 2002.

[7] T. Theofanous, C. Liu, S. Additon, S. Angelini and O. Kymiliinen, "In-vessel coolability and retention of a core melt," *Nuclear Engineering and Design (1997) 1 48,* vol. 169, pp. 1-48, 1997.

[8] T. Theofanous, M. Maguire, S. Angelini and T. Salmassi, ""The first results from the ACOPO experiment"," *Nuclear Engineering and Design,* vol. 169 , pp. 49-57, 1997 ACOPO.

[9] X. Gaus-Liu, A. Miassoedov, T. Cron, B. Fluhrer, S. Schmidt-Stiefel and T. Wenz, "test and simulation results of LIVE-L4 +LIVE-L5L", KIT Scientific publishing, 2011.

[10] B. Fluhrer, A. Miasoedov, X. Gaus-Liu and T. Cron, "Experiement in the LIVE-2D test facility at KIT on melt behavior in RPV lower head," in *Nureth15*, 2013.

[11] X. Gaus-Liu, B. Fluhrer, T. Cron and T. Wenz, "First results in the LIVE-2D test facility at KIT on melt behaviour in RPV lower head," in *Jahrestagung Kerntechnik*, Stuttgart, 2011.

[12] F. Kretzschmar and B. Fluhrer, "Behavior of the Melt Pool in the Lower Plenum of the Reactor Pressure Vessel -Review of Experimental Programs and Background of the LIVE Program," Forschungszentrum Karlsruhe, 2008.

[13] A. Miassoedov, T. Cron, J. Foit, X. Gaus-Liu, S. Schmidt-Stiefel and T. Wenz, "LIVE-experiments on melt behavior in the RPV lower head.," in *Proceedings ICONE-16*, Orlando, 2008.

[14] X. Gaus-Liu, A. Miassoedov, J. Foit, T. Cron, F. Kretzschmar, A. W. T. Palagin and S.-S. S., "LIVE-L4 and LIVE-L5L Experiments on Melt Pool and Crust Behavior in Lower Head of Reactor Pressure Vessel," *Nuclear Technology,* Vol. 181, Nr.1, pp. 216-226, 2013.

[15] X. Gaus-Liu and A. Miassoedov, "LIVE Experimental results of melt pool behaviour in the PWR lower head with insulated upper lid and exernal cooling," in *ICONE21*, Chengdu, 2013.

[16] X. Gaus-Liu, A. Miassoedov, B. Fluhrer, T. Cron, J. Foit, S. Schmidt-Stiefel and T. Wenz, "KIT Scientific report 7542"Results of the LIVE-L3A Experiment"," KIT Scientific publishing, Karlsruhe, 2010.

[17] B. Sehgal and Z. Yang, "Ex-Vessel Core Melt Stabilization Research: On the Experiments with Simulant Materials at KTH," KTH, Stockholm, Sweden, 2001.

[18] F. Asfia and V. Dhir, "An experimental study of natural convection in a volumetrically heated spherical pool bounded on top with a rigid wall," *Nuclear Engineering and Design,* vol. 163, pp. 333-348, 1996.

[19] F. Mayinger, M. Jahn, H. Reineke and U. Steinberner, "Untersuchung thermohydraulischer Vorgänge sowie Wärmeaustausch in der Kernschmelze," Bundesministerium für Forschung und Technologie, 1975.

[20] B. R. Sehgal, "Nuclear safety in light water reactors", Elsevier, ISBN: 978-0-12-388446-6, 2012, p. 136.

[21] X. Gaus-Liu, A. Miassoedov, T. Cron, S. Schmidt-Stiefel und T. Wenz, „LIVE-L8B test - Debris melting process," SARNET2-COOL-P06, 2011.